J. Am. Soc. Mass Spectrom. (2016) 27:897–907
DOI: 10.1007/s13361-016-1354-8

RESEARCH ARTICLE

Multimodal Vacuum-Assisted Plasma Ion (VaPI) Source with Transmission Mode and Laser Ablation Sampling Capabilities

Joel D. Keelor,[1] Paul B. Farnsworth,[2] Arthur L. Weber,[3] Heather Abbott-Lyon,[4] Facundo M. Fernández[1]

[1]School of Chemistry and Biochemistry, Georgia Institute of Technology, Atlanta, GA 30332, USA
[2]Department of Chemistry and Biochemistry, Brigham Young University, Provo, UT 84602, USA
[3]SETI Institute, Mountain View, CA 94043, USA
[4]Department of Chemistry and Biochemistry, Kennesaw State University, Kennesaw, GA 30144, USA

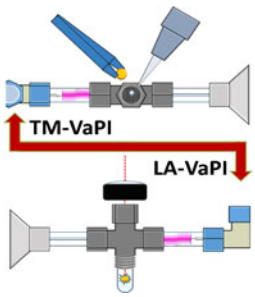

Abstract. We have developed a multimodal ion source design that can be configured on the fly for various analysis modes, designed for more efficient and reproducible sampling at the mass spectrometer atmospheric pressure (AP) interface in a number of different applications. This vacuum-assisted plasma ionization (VaPI) source features interchangeable transmission mode and laser ablation sampling geometries. Operating in both AC and DC power regimes with similar results, the ion source was optimized for parameters including helium flow rate and gas temperature using transmission mode to analyze volatile standards and drug tablets. Using laser ablation, matrix effects were studied, and the source was used to monitor the products of model prebiotic synthetic reactions.

Keywords: Ambient plasma ionization, Mass spectrometry, Transmission mode, Laser ablation, Prebiotic chemistry

Received: 18 September 2015/Revised: 22 January 2016/Accepted: 25 January 2016/Published Online: 16 February 2016

Introduction

Ambient plasma-discharge ionization continues to be a burgeoning field in mass spectrometry. Since direct analysis in real time (DART) was reported in 2005 by Cody et al. [1], a variety of different plasma ionization technologies have been developed, most notable examples including low temperature plasma (LTP) [2], plasma-assisted desorption ionization (PADI) [3, 4], and flowing atmospheric pressure afterglow (FAPA) [5, 6]. Plasma ion sources have garnered wide acceptance and demonstrated utility for routine detection of small molecules in homeland security and forensic applications [7, 8], environmental [9, 10] and reaction monitoring [11], food [9, 12] and drug quality analysis [13–15], and more recently in metabolic fingerprinting for diagnostic applications [16, 17]. Performance has been shown to be comparable between different source constructs, with unique plasma characteristics principally dictated by device dimensions, power regime (AC or DC), and discharge gases used [18, 19]. The currently understood glow discharge ionization mechanisms and physiochemical variables influencing ionization efficiency have been summarized elsewhere in detail [20, 21].

Ambient fluid dynamics at the spectrometer inlet significantly impact ion transmission and can be difficult to control. Reproducible sampling and quantitation with plasma discharge sources have proven to be complicated, necessitating the use of internal standards [22, 23] and automated sampling approaches [24]. Much effort has been dedicated to improving the sensitivity and sampling efficiency of these ionization techniques with the aid of simulations that model gas flow patterns [25, 26] and real-time visualization of source gas flow profiles using the Schlieren technique [27–29]. The most successful attempts at enhancing the quantitative capability of ambient plasma-based analysis have been realized with DART-MS systems

Electronic supplementary material The online version of this article (doi:10.1007/s13361-016-1354-8) contains supplementary material, which is available to authorized users.

Correspondence to: Facundo M. Fernández;
e-mail: facundo.fernandez@chemistry.gatech.edu

incorporating a Vapur interface, rail-mounted sampling probes, and auxiliary pumping, all of which help entrain divergent gas flows toward the mass spectrometer inlet and reduce variability [30]. More recently, continuous quantitative surface scanning with DART has been accomplished using planar substrates in place of capillary holders [31].

Spatial resolution for plasma ion sources, affected by sample size and shape, is typically limited by dispersive gas-flow dynamics. One successful strategy used to improve spatial resolution has been coupling of plasma ionization with laser ablation, wherein high-energy laser pulses desorb neutral material with micron spatial resolution. For example, laser ablation has been paired successfully with dielectric-barrier-discharges (DBD) [32] to examine nonvolatile explosives, and used with DART [33] and FAPA [34] for imaging mass spectrometry of biological tissues, dyes, and drugs. In these approaches, the substrate radiation absorption efficiency and ablation plume expansion remain the limiting factors determining the abundance of aerosolized sample available for ionization, while the plasma ion current and source gas-flow fidelity dictate the ion generation and transmission efficiencies, respectively.

The increasingly more accessible mass spectrometer AP interfaces continue to enable new sample introduction modes that alleviate ion losses related to mass transport. For example, vacuum-assisted sampling has been coupled with rf plasma discharges within or directly connected to the inlet transfer capillary [35–37]. Such sampling approaches function as aerodynamic remote sampling stages similar to the remote analyte sampling, transport, and ionization (RASTIR) [38] idea implemented with extractive electrospray ionization (EESI).

Drawing inspiration from these AP sampling techniques and several methodologies established in the same vein, including electrothermal vaporization (ETV)-DART [39] or Drop-on-Demand FAPA [40], we present a multimodal plasma ion source named vacuum-assisted plasma ionization (VaPI) that integrates laser ablation and transmission mode sampling with AC/DC plasma ionization mass spectrometry. The core component of this new ion source architecture is a central cross union bridging a plasma discharge cell to the mass spectrometer transfer capillary in a coaxial orientation. Open cross bridge joints are interchangeably adapted with either a mesh sample screen for transmission mode analysis (TM-VaPI) or sealed with a sapphire window permitting focused laser throughput for ablation experiments (LA-VaPI). The suction of the mass spectrometer is partially maintained within the cross union when using helium discharge gas, thereby allowing material to be drawn into the source, improving sampling consistency. With increasing plasma power and concomitant rising cell temperature, the union serves as an incubated vessel facilitating analyte desolvation and mixing, as well as efficient ionization and transmission. Optimal settings for co-dependent variables affecting ionization efficiency and transmission, namely helium gas flow rate, cell temperature, and plasma power, have been determined. Effects of matrix composition were also investigated, showcasing VaPI's robust tolerance to sample complexity. The best sample delivery practices to ensure sampling reproducibility are also discussed.

Experimental

Materials and Sample Preparation

Reagent grade dimethyl methylphosphonate [DMMP] and 2,4-lutidine were purchased from Sigma-Aldrich (St. Louis, MO, USA) and prepared as aqueous solutions by serial dilution in concentrations of 6.25, 12.5, 25, 50, 100, and 200 μM from a 1 mM stock solution. An analytical grade standard mixture of amino acids was also procured from Sigma-Aldrich and used without further preparation. The mixture concentration was 2.5 μmol mL^{-1} in 0.1 N HCl for all components unless otherwise specified, and consisted of L-alanine, ammonium chloride, L-asparagine, L-aspartic acid, L-cystine (1.25 μmol mL^{-1}), L-glutamic acid, glycine, L-histidine, L-isoleucine, L-leucine, L-lysine, L-methionine, L-phenylalanine, L-proline, L-serine, L-threonine, L-tyrosine, and L-valine. Triaminopyrimidine [TAP] (Acros Organics, part of Thermo Fisher Scientific Inc., NJ, USA) was made into 2.5 mM aqueous solutions mixed with potassium chloride (J.T. Baker brand from Avantor Performance Materials, Center Valley, PA, USA) using salt concentrations of 5, 10, 20, and 40 mM KCl. Poly(ethylene) glycol [M_n 395, M_w 430] from American Polymer Standards Corporation (Mentor, OH, USA) was dissolved into ~4 mg mL^{-1} aqueous solutions with solvent compositions of 0%, 20%, 50%, and 90% volume methanol (LC-MS grade, Sigma-Aldrich).

Drug tablet samples included acetaminophen [500 mg] sold by Target, Inc. (Minneapolis, MN, USA), Doralgine [25/500 mg caffeine/noramidopyrine] made by Medical Supply Company, Ltd. (Phnom Penh, Cambodia), and Coartem [20/120 mg artemether/lumefantrine] from Novartis AG Pharmaceutical Company (Suffern, NY, USA).

Synthetic nucleobase mixtures were produced from two separate model prebiotic reactions. Purine and pyrimidine compounds were synthesized in the formamide reaction. A ~5 mL volume of formamide (reagent grade, Sigma-Aldrich) was heated in an oven at 160 °C for up to 120 h in a 20-mL scintillation vial covered with foil. Fractions of the reaction mixture were collected at 72 and 120 h time points and stored at 8 °C for 24 h before workup. Reacted formamide mixture aliquots of 100 μL or ~120 mg were dissolved in 10 mL of deionized water and filtered through a 0.45 μm PTFE membrane before analysis. Pyrazine derivatives were synthesized from a one-pot reaction, in which 1,3-dihydroxyacetone, glycolaldehyde, and 2-aminoacetamidine-dihydrobromide (0.10 M 1:1:1 ratio) were mixed in aqueous solution with sodium phosphate (0.25 M) at pH 7.4 by addition of NaOH, then heated to 85 °C for 24 h. In a 2-mL microvial, reaction contents were de-aerated and purged with nitrogen before being sealed under vacuum. A 1.0 mL aliquot of the product mixture was diluted with 8 mL of water, and a 5 mL portion was then desalted on a 20 mL Discovery DSC-18 column (Supelco, Bellefonte, PA, USA). Material was eluted with 36 mL water and 44 mL 50% methanol/water,

collected in 20 separate fractions. Salt-free fractions #10-20 (from 37-80 mL eluent) were combined and concentrated to 0.5 mL syrup using a CentriVap centrifuge. After storage at –20 °C, the mixture was suspended in 200 µL water, and 50 µL aliquots were further diluted in 300 µL water for adequate ampoule sampling volume.

Deionized water was generated with a Barnstead Nanopure Diamond laboratory water system (Thermo Fisher Scientific, Inc.) and ultrapure (99.999%) helium source gas was supplied by Airgas (Atlanta, GA, USA).

VaPI Plasma Ion Source Design and Operation

The custom plasma discharge source was fashioned from a quarter-inch PFA Swagelok (Solon, OH, USA) T-junction securing a quartz tube (l = 50 mm, o.d. = 6.25 mm, i.d. = 3.95 mm) that enclosed a tungsten needle electrode (l = 120 mm, diameter = 1 mm) at one joint opening. The point electrode was center-mounted in a perforated ceramic piece (dia.meter = 3.95 mm) inserted at the base of the quartz tube, and the electrode rod extended within the T-junction body through a Teflon plug capping the opposite joint. A gas feed line was fitted in the top opening. The quartz tube terminated at an eighth-inch metal ferrule (grounded counter-electrode) in a stainless steel quarter-inch Swagelok cross union, which was connected on-axis with the mass spectrometer via a truncated glass transfer capillary (l = 40 mm, o.d. = 6.35 mm, i.d. = 500 µm) from Bruker (Billerica, MA, USA). The Swagelok cross union body was wrapped in 1 ft. high-temperature heating cord (22 W) with a J-type thermocouple, allowing temperature to be regulated using an SDC digital temperature controller (Briskheat, Columbus, OH, USA). High-temperature quarter-inch 60%/40% vespel/graphite ferrules (Restek, Bellefonte, PA, USA) were used at all Swagelok joint connections. Thermal images of the plasma source and cross unit were collected with a FLIR T300 IR camera (FLIR Systems AB, Danderyd, Sweden).

The electric discharge was operated at powers of ~20 ± 1 W in both AC and DC regimes using helium source gas. In DC mode, a negative potential bias of ~2500 V was applied to the tungsten needle in series with 50 kΩ ballast resistor using a Bertan Associates 205A-50R HV power supply (Bertan Associates Inc., Hicksville, NY, USA). The effective DC electrode potential and current measured with a HV probe were ~1850 V and ~11 mA, respectively. For AC mode, power was applied to the tungsten needle from a T&C Power Conversion AG-0201A rf power supply (T&C Power Conversion Inc., Rochester, NY, USA). Plasma power was estimated from the difference between effective load powers ($P_{Load} = P_{Forward} - P_{Reverse}$) with the discharge on and off. AC electrode potentials of ~1240–1460 V_{rms} were measured on an oscilloscope (Tektronix, Beaverton, OR, USA), with I_{rms} estimated between 13 and 16 mA for a 20 W AC discharge. Helium flow rates were controlled between 1.0 and 2.0 LPM using an analog rotameter (Aalborg, Orangeburg, NY, USA) in-line with an M series digital flow meter (Alicat Scientific, Tuscon, AZ, USA). Vacuum pressure within the cross union was estimated with a DM8320 digital manometer (General Tools, Secaucus, NJ, USA) fastened on one open joint while keeping the others sealed.

Instrumentation and Sampling Methods

For transmission mode geometry sampling, a 40 × 40 stainless steel mesh screen (diameter = 9.35 mm) was fastened in the top cross union opening of the VaPI ion source and the lower union opening was kept sealed. During ion source characterization, volatile compounds were sampled from a strictly aqueous matrix to reduce spectral complexity. The droplet water introduced during sampling would only contribute to the $(H_2O)_nH^+$ reactant ion population, thereby preventing the possibility of ion competition with an organic solvent. Solutions were spotted onto the mesh in 3 µL aliquots using a micropipette. For solids analysis, drug tablet fragments were placed atop the mesh with tweezers for approximately 1 min, and then removed. If needed, methanol solvent or water was spotted in aliquots of 10–100 µL to rinse the mesh.

When sampling by laser ablation, the bottom union inlet was left open and a sapphire window (h = 1 mm, diameter = 9.35 mm) was fastened in the top joint. Laser ablation was performed using an IR Opolette OPO laser model 2731 (Opotek, Inc., Carlsbad, CA, USA). Laser wavelength and frequency were tuned to 2940 nm and 10 Hz, respectively. Laser energy was tuned to 88.1%, equating to an output energy of ~1.55 mJ measured with an ES111C pyroelectric sensor (Thorlabs, Inc., Newton, NJ, USA), focused by a MgF_2 plano-convex lens (*f.l.* 5 cm) through the Swagelok cross union. Ablation of sample solution was conducted from 10 µL droplets deposited on an Omni slide glass substrate with Teflon-coated spot arrays (Prosolia, Indianapolis, IN, USA), or from a 200 µL reservoir of solution contained in a quarter-inch quartz ampoule. Unless otherwise specified, all ablation was performed from aqueous solutions. Laser ablation was also performed using an open AP interface arrangement during a comparison study. In place of the cross union bridge unit, the discharge source was capped with a quarter-inch Swagelok end fitting as the grounded counter electrode and positioned ~0.5 cm away from the spectrometer capillary inlet. The planar Omni slide substrate was mounted on a guide arm extending from a *xyz* stage, and centered below the spectrometer inlet in the interface flush underneath the plasma endcap electrode.

All experiments were conducted on a JEOL JMS-T100LC AccuTOF mass spectrometer (JEOL USA, Inc., Peabody, MA, USA) using the following positive mode tune parameters optimized for the low mass range — orifice #1: 25 V, orifice #2: 5 V, ring lens: 10 V, orifice temperature: 100 °C; ion guide rf voltage: 100–400 V, sweep time: 80%; guide bias voltage: 29 V, pusher bias voltage: –0.28 V, MCP detector: 2650 V. In most cases, nominal masses are reported for known compound peaks, but for unknown species, assigned ion formulas were deduced from the accurate masses provided in the text.

Results and Discussion

TM-VaPI Characterization

A schematic illustration of the VaPI source assembly is depicted in Figure 1, with corresponding pictures presented in Supplementary Figure S1a, b (in supporting information). The source configuration in Figure 1a, intended for transmission mode analysis, features a mesh sample screen on the top cross union joint. A steady draw of air flows into the cross union through the sample mesh, driven by the suction from the spectrometer inlet and modulated by helium flow rate and cell temperature. This source design mitigates the unfavorable fluid dynamics of open format (ambient) plasma ion sources, with the focused vacuum draw through the mesh improving sensitivity by affording more complete entrainment of volatilized sample into the plasma gas. With this setup, an elevated plasma gas temperature was necessary not only to initiate analyte thermal desorption but also to enhance analyte cluster desolvation and minimize condensation on the interior cell surface. Accordingly, glow discharges were operated at target powers of ~20 W, where helium gas temperatures measured with a thermocouple reached 200 °C in the cross union without the addition of extra heating elements.

Aqueous solutions of 2,4-lutidine and DMMP were sampled first to determine general performance and dynamic range while optimizing for helium gas flow rate and cell temperature. When microliter aliquots of solution were spotted onto the screen, the droplet was slowly aspirated into the cross union, mixing in the afterglow helium stream. Volatile analytes were initially chosen for characterization experiments to avoid carryover that might skew trends. Supplementary Figure S2a shows the highly repeatable extracted ion chronograms for the protonated monomer of 2,4-lutidine in a concentration series, and Supplementary Figure S2b displays a select subset of extracted ion chronograms for the DMMP protonated monomer and dimer detected from a 50 μM solution. Differences in desorption profile shapes were observed based on analyte volatility. For instance, the desorption profile for DMMP suggested a lower volatility from the droplet surface, indicated by the gradual rise to a maximum and subsequently sharp decrease to baseline upon depletion of the droplet, compared with the more volatile 2,4-lutidine, the peak profile of which showed an inverse trend. Furthermore, as it is apparent in Supplementary Figure S2b, the DMMP dimer peak emerged later than the monomer, appearing only after concentration by the shrinking droplet. These observations were compatible with DMMP's slightly higher enthalpy of vaporization and boiling point. Meanwhile, no dimer ion was observed for the more rapidly volatilized 2,4-lutdine even at 1 mM solution concentrations. However, a minor ion suspected to form through a pyridine N-oxide intermediate did appear at higher 2,4-lutidine concentrations, with the formula $[C_7H_8NO]^+$ assigned by accurate mass ($m/z = 122.0628$). The origin of this and other product ions is discussed in following sections.

The cross union pressure and vacuum draw were largely influenced by the plasma helium flow rate and cell union temperature, which in turn impacted sampling reproducibility and sensitivity for TM-VaPI. Figure 2a shows the signal intensity as a function of helium flow rate for aliquots of DMMP and 2,4-lutidine spotted on the mesh. When the glow discharge was active, the cross union vacuum pressure measured between –116 mmHg at 1.0 LPM helium to –13 mmHg at 1.8 LPM helium. A plot of relative cross union pressure (normalized to a percentage) as a function of flow rate and temperature can be found in Supplementary Figure S3. Signal was seen to increase for each analyte with helium flow rates up to ~1.6 LPM (cell pressure: –40 mmHg) due to a higher flux of plasma species into the VaPI cross joint available to sustain ionization

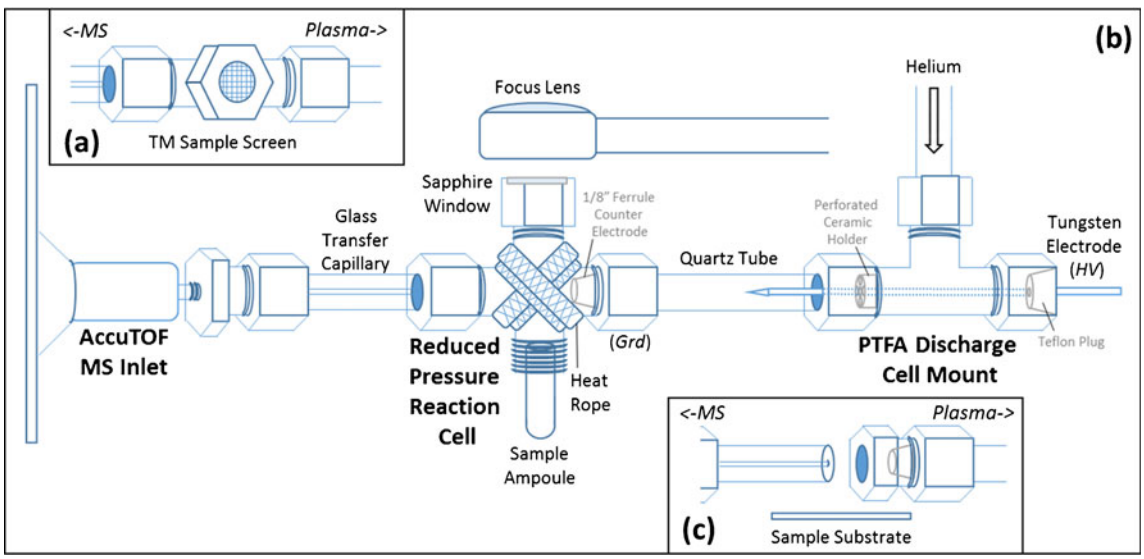

Figure 1. Schematic of vacuum-assisted plasma ionization (VaPI) source assembly. Configuration used for transmission mode (TM)-VaPI sampling **(a)**. Configuration used for laser ablation (LA)-VaPI sampling **(b)**. Open atmospheric pressure interface arrangement with plasma source **(c)**

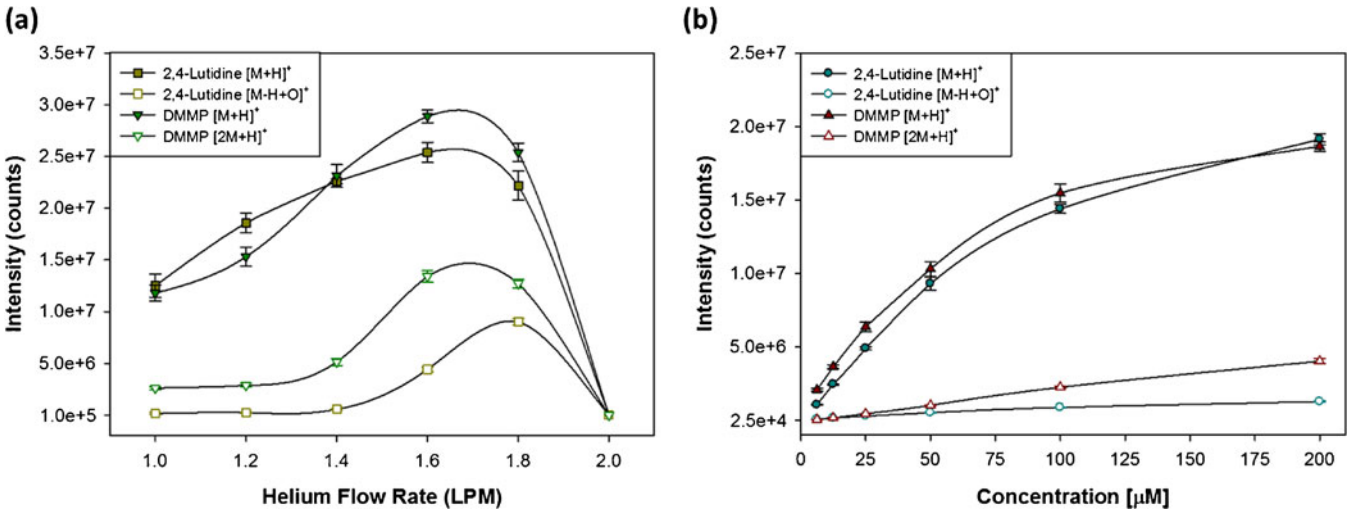

Figure 2. Signal intensities as a function of source gas flow rate **(a)** and volatile standard concentration **(b)** for 2,4-lutidine and DMMP using TM-VaPI with a 20 W DC discharge. Data points and standard deviation error bars represent the average extracted TIC areas for three consecutive peak traces per point in **(a)** and five consecutive peak traces per point in **(b)**

reactions. The high intensity of reactant protonated water clusters persisted for helium flow rates over 2.0 LPM, but measured analyte signal rapidly disappeared with flow rates beyond 1.8 LPM helium. This result was the consequence of a now positive pressure at the mesh (≥15 mmHg), which effectively negated suction and suppressed transmission of desorbed neutrals. Additionally, the flood of hot gas into the cross union when using these higher helium flow rates also heated the mesh, likely accelerating some sample evaporation into the environment, thereby contributing to signal loss. Newer, more sensitive mass analyzers with vacuum systems less robust to high helium gas loads could potentially operate VaPI at far lower flow rates or use reduced cell assembly dimensions, thereby maximizing vacuum draw for improved sample uptake and ion transmission without much compromise to ionization efficiency.

The VaPI linear range was also examined via concentration series for each standard, Figure 2b. The increasing signal intensity deviated from linearity after the concentration range spanned three orders of magnitude, with the protonated ion signals beginning to plateau at around 100 μM (see Supplementary Figure S4 for this trend forecast using total ion signal with AC/DC plasmas.) Interestingly, the protonated water population was not fully consumed even at higher analyte concentrations, an observation suggesting that fluid dynamics and ionization reaction kinetics rather than reactant ion depletion are likely the limiting factors. It is reasoned that evaporative losses from the slowly aspirating micro-droplets are more significant at higher volatile concentrations, and dynamic range linearity may be restored by either amplifying VaPI vacuum pressure or sealing off the sample mesh after spotting. The %RSD for volatile standards in Figure 2 still never exceeded ±8%, and was under ±2% for the majority of data points.

Where sensitivity was not an issue, that sampling reproducibility could be further improved by controlling cell temperature. Material aspirated through the sample mesh partially cools the afterglow gas while mixing in the cross union, disrupting the gas flow profile and vacuum equilibrium to cause temporary fluctuations in the total ion chronogram. With heating rope wrapped around the cross union and programmed to 275 °C, the extracted ion chronogram shapes for each standard appeared more smooth and narrow (Figure 3) compared with TIC peaks at lower temperatures, with the standard deviation decreasing more than 2-fold. However, this improvement came at the expense of lower sensitivity for the volatile analyte, with the average integrated signal intensity for DMMP being reduced by almost half. The signal decrease in response to excessively heating the cell is easily rationalized. Higher temperatures accelerated sample desorption from the mesh while simultaneously reducing the net vacuum pull. A near total loss of cross union vacuum pressure (–2 mmHg) was actually measured at 1.6 LPM and 275 °C, indicating signal under these

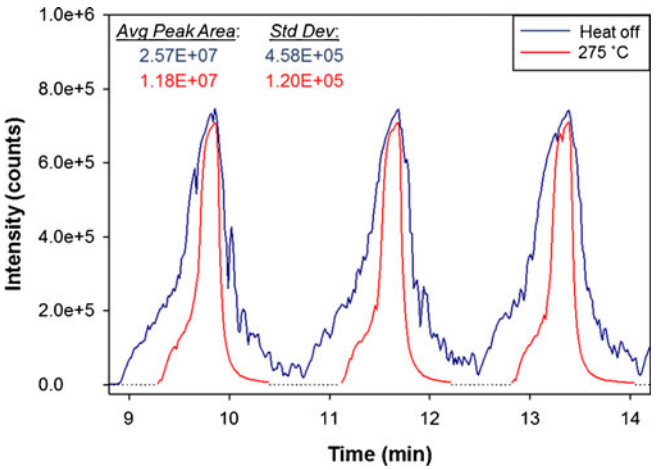

Figure 3. Extracted ion peak traces for 1 mM DMMP at 1.6 LPM helium flow rate with (**red**) and without (**blue**) the cross union heated to 275 °C. (Baseline/time axis for superimposed consecutive red traces were altered to fit blue trace)

conditions may have depended almost solely on analyte diffusion into the cell. As will be seen in the next section, such temperature effects also manifest themselves as differences in performance between AC and DC plasma power regimes. Since setting the cross union temperature to match the temperature of the discharge gas minimizes hysteresis during sampling, the cross union temperature was set to 200 °C where vacuum draw was preserved.

Comparison of AC and DC VaPI Operation Modes

A recent study involving high-frequency DBD plasmas and point-to-plane glow discharges presented spectroscopic evidence suggesting the abundance of helium metastables varies considerably for different plasma ion source geometries, and between AC or DC operation modes [41]. Metastable atom concentration within a plasma was seen to scale proportionally with plasma power, with lower wattage (10–15 W) DBDs generating He* populations up to an order of magnitude larger than those observed for higher power FAPA-type DC discharges. In principle, a greater number of plasma metastable species should be followed by a higher population of reactant ions in the AP interface and possibly higher ionization efficiency. Given the reproducible, semiquantitative capabilities of TM-VaPI, AC and DC discharges were tested in order to investigate the downstream implications of the spectroscopic findings, and to determine any performance advantage.

At first glance, the plasma discharges appeared visually distinct for a given mode; the AC discharge existing as a pink, focused plasma and the DC discharge as a more diffuse, white glow. Signal trends observed as a function of helium flow rate and concentration were almost identical between both power regimes (Supplementary Figures S5a, b). For comparison, analyte ion intensity ratios for the discharge modes (DC/AC) are tabulated in Supplementary Figure S5c. Signal intensity gradually shifted in favor of the DC discharge from ≥0.75 times to over 1.5 times the total AC ion count as the helium flow rate was increased. Additionally, the signal gain for the DC discharge slowly diminished from around 2 to 1.3 times the AC ion intensity as analyte concentration increased. The overall lower signal for the AC plasma in most cases is difficult to rationalize based on the previously measured metastable densities. Apart from plasma visual appearance, the major observable difference between the two discharges was the VaPI cell temperature. In Supplementary Figure S6, thermal images of the source recorded using different helium flow rates showed temperatures approximately 20 °C higher for AC versus DC operation, as might be expected because of the 2–3 mA larger plasma current calculated for the AC discharge. Recalling the effect of raised gas and cross union temperatures on signal described previously using this configuration, it is likely that this small temperature disparity between power modes was predominantly responsible for decreased ion transmission and lower volatile signal intensity in AC mode.

On average, the protonated water cluster population detected for the AC plasma was comparable to that of the DC mode discharge, with the net water ion signal consistently equal or only marginally higher. Even with VaPI parameters optimized, the largest $(H_2O_nH)^+$ signal advantage witnessed for AC mode was <2.5-fold intensity over DC mode, still significantly less than the order of magnitude higher concentration that could be expected from metastable atom spectroscopy. Interestingly, protonated water clusters were observed even when all cross union openings of the VaPI ion source were sealed off from the atmosphere. This finding suggests reactant ions were formed in the discharge from plasma gas impurities and not just He* Penning ionization of ambient air molecules. More substantive conclusions may be reached by comparing plasmas in AC/DC power regimes using even higher quality gases while controlling system temperature. Ultimately, since the DC discharge offered more stable operation and simpler *I/V* control, it was selected over AC mode for continued experiments.

TM-VaPI Analysis of Solids

Based on the characterization experiments with volatile standards, the TM-VaPI ion source is potentially well-suited to MS applications that require rapid qualitative and semiquantitative analysis, such as composition screening, reaction monitoring, and molecular profiling. Using the default transmission mode geometry, the ion source was amenable to sampling solids without protracted analyte extraction/dissolution steps. Fragment pieces from a variety of pharmaceutical tablets were placed on the cross union sample mesh and a stable signal trace could be achieved (Supplementary Figure S7). Absolute ion intensity and relative distribution for tablet active ingredients was again found to depend on both helium flow rate and plasma temperature, with less detriment than when sampling volatiles. Desorption and ionization could be effectively tuned to favor different target analytes by raising the cross union temperature. Cross union temperature was maintained at approximately 275 °C, where thermal desorption for heavier compounds from a solid matrix was efficient, but below the temperature limit where poor fluid dynamics and vacuum loss occurred. For a few select cases, it was found that higher sensitivity was obtained when organic solvent was spotted on the mesh immediately after removing the larger tablet fragments.

The spectrum for a single component drug tablet containing acetaminophen (500 mg) is shown in Supplementary Figure S8a. Interestingly, both the molecular ion and protonated species were detected. The afterglow of the 20 W DC plasma (~200 °C) was sufficient to thermally desorb the compound and provide ample signal, but a noticeable 20%–25% increase in total acetaminophen ion intensity was observed when heating the cross union to 275 °C, Supplementary Figure S8b. As expected, the elevated cross union temperature served to enhance desorption off the mesh and cross union interior walls, resulting in a stable $[M+H]^+$ intensity but now a more abundant $[2M+H]^+$ species. A similar effect was seen for Doralgine tablets containing both caffeine (25 mg) and noramidopyrine (120 mg), and example spectra are shown here

in Figure 4. Without external heating, the spectrum featured primarily the $[M+H]^+$ ions of both ingredients, with caffeine being the most abundant, Figure 4a. Again, $M^{+\cdot}$ molecular ions of both compounds were also observed. Raising the cross union temperature to 275 °C had a dramatic effect, where the signal for caffeine was quickly dwarfed and the protonated monomer and dimer peaks of the more concentrated noramidopyrine ingredient dominated the spectrum with an ~4-fold signal increase, Figure 4b. The smaller peaks neighboring the noramidopyrine signals suggest the inclusion of dipyrone and/or metamizole analogues as lesser tablet constituents, having formulas matching a metamizole protonated fragment ion $[C_{13}H_{17}N_3O+H]^+$ ($m/z = 232.1427$) and noramidopyrine/dipyrone fragment dimer complex $[(C_{13}H_{16}N_3O)(C_{12}H_{15}N_3O)]^+$ ($m/z = 447.2500$). For both tablets, the increased abundance of dimer species is attributed to a rise in the overall analyte vapor pressure with higher VaPI cell temperatures and also partial cooling/clustering of the volatilized analyte in the transfer capillary.

Antimalarial Coartem tablets containing higher mass artemether (20 mg) and lumefantrine (80 mg) ingredients were sampled as well, employing additional sample treatment to improve analysis. Compounds in the artemisinin family are prone to fragmentation during both electrospray and plasma ionization, and in Supplementary Figure S8c, the characteristic ion fragments for artemether are readily seen at $m/z = 163$, 221, 267, and 281 as previously identified in the literature [42]. Heating the cross union to 275 °C only shifted the relative intensities of the observed species in greater favor of fragments at $m/z = 221$ and a lesser fragment at $m/z = 253$ (spectrum not shown), but otherwise did not alter the total ion signal distribution. Detection of the heavier lumefantrine ingredient required addition of organic solvent to the mesh, Supplementary Figure S8d. It is speculated that the solvent vapor acted as a sort of extractant, similar to a codistillation process, where the boiled solvent wetted tablet residue and freed material condensate adhering to the mesh or cross union walls. Upon removal of the tablet pieces and addition of methanol in microliter aliquots to the mesh screen, the protonated lumefantrine monomer with its chlorine isotopes appeared at $m/z = 528$ and m/z = 530, accompanied by more intense peaks in the low mass range. These peaks are associated with $M^{+\cdot}$ fragments of lumefantrine formed by cleavage of the amine moiety and are identified based on accurate mass as $[C_8H_{18}N]^+$ ($m/z = 128.1449$) and $[C_9H_{20}N]^+$ ($m/z = 142.1604$). The observation of $M^{+\cdot}$ ions in addition to $[nM+H]^+$ is not entirely unexpected, considering the analyte direct exposure to the highly energetic afterglow reactive species.

LA-VaPI Characterization

Typical LA-plasma ion source configurations reported in the literature make use of an open format where fluid dynamic effects at the mass spectrometer inlet result in significant ion transmission losses. To investigate if the more controlled sampling capabilities of VaPI could further enhance LA-plasma ionization approaches, we tested a LA-VaPI configuration, as depicted in Figure 1b. Performance of the vacuum-assisted LA-VaPI source design compared with an optimized open air configuration (Figure 1c) is presented in Figure 5. An amino acid standard mixture was analyzed by laser ablation of microliter droplets deposited between Teflon spots on a glass slide. Tentative peak assignments were made for 15 of the 17 mixture components. Judging by the spectral distribution, ionization appeared to be decided by compound hydrophobicity and enthalpy of vaporization rather than gas-phase basicity, favoring amino acids with higher surface activity and evaporation rates over those with the greatest side-chain proton affinity. The exception relative to the other undetected basic and hydrophilic amino acids was proline, primed to dominate the spectrum owing to a higher predicted volatility over species like histidine and a rigid structure better able to withstand the energy of glow discharge ionization compared with the more fragile arginine [43]. The amino acid ion populations observed were very similar across spectra for both source configurations, but signal

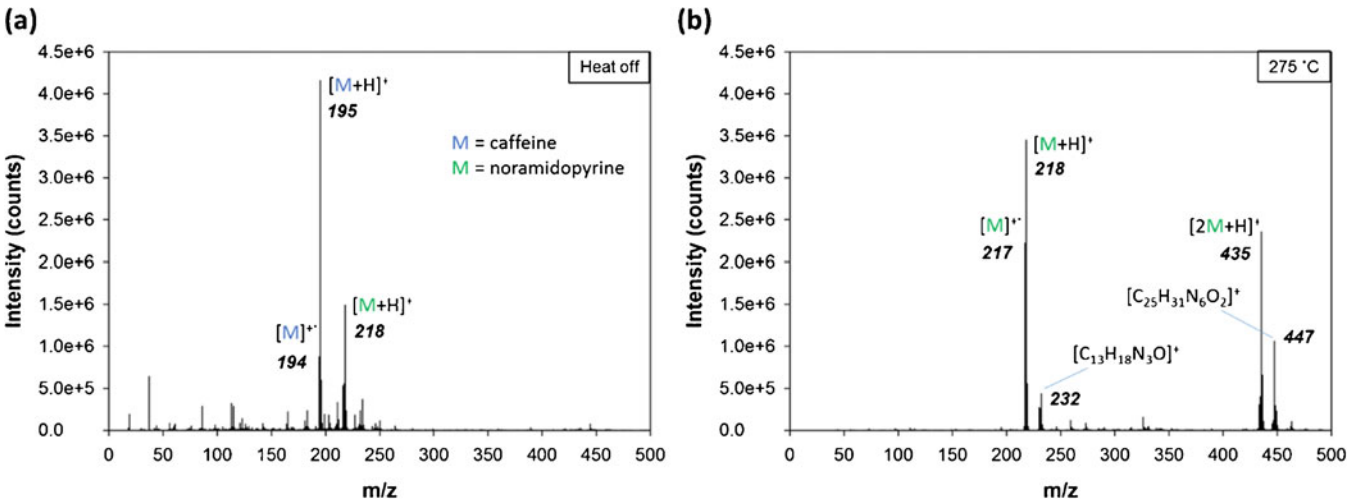

Figure 4. Mass spectra for a Doralgine drug tablet fragment collected by TM-VaPI using 20 W DC discharge and 1.6 LPM helium **(a)** and with cross union heated to 275 °C **(b)**. Spectra were derived from 30 s averages of the TIC signal for each tablet

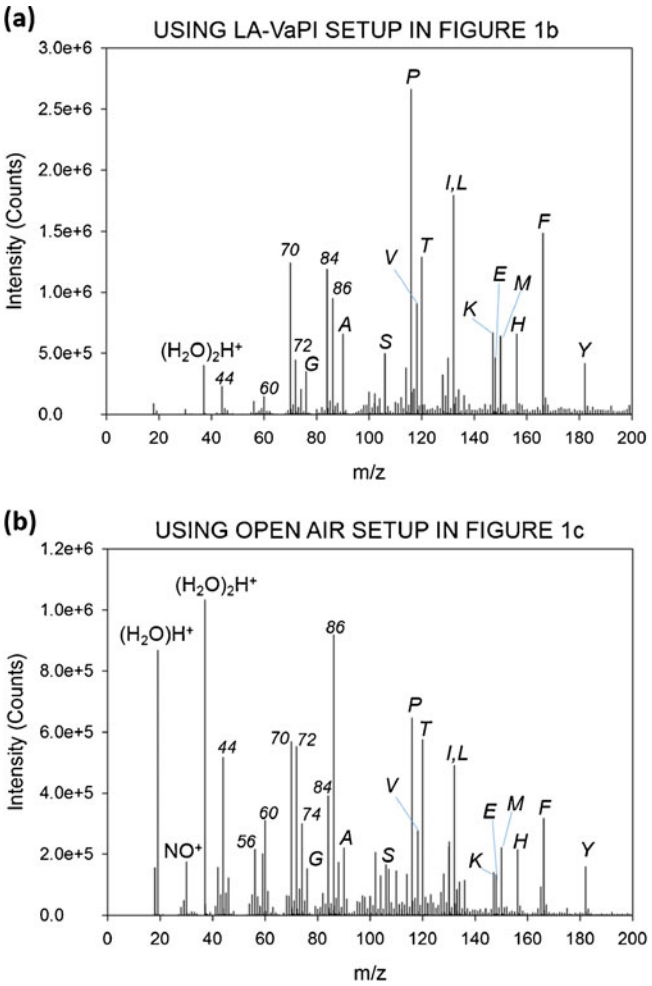

Figure 5. Mass spectra of 2.5 mM amino acid standard in 0.1 N HCl sampled by laser ablation and plasma ionization using either the LA-VaPI scheme from Figure 1b **(a)** or a traditional open AP interface arrangement shown in Figure 1c **(b)**. Standard mixture was ablated from 10 µL droplet on Omni slide substrate. Spectra are an average of full time until droplets were consumed (~20 s each). Laser wavelength, frequency, and effective energy were 2940 nm, 10 Hz, and ~1 mJ. Optimal helium flow rate for **(a)** was 1.6 LPM and 1.3 LPM for **(b)** with the cross union heated to ~200 °C

intensities were superior using the LA-VaPI scheme shown in Figure 1b. Total signal intensity was ≥2.5 times higher for all amino acids detected (Figure 5a) and the protonated reactant water clusters were almost completely consumed. In contrast, many of the reactant ions were seen to survive in the spectrum for the open interface LA-plasma source arrangement, Figure 5b. As observed previously using a VaPI configuration, ambient air suctioned through the inlet partly cooled the plasma gas. This effect in combination with the enclosed nature of the VaPI ion source also helped reduce spectral complexity in the low mass range, signified by fewer amino acid fragment ions appearing under 100 Da (Figure 5b).

Following these LA-VaPI experiments, an alternative sampling approach was tested with the goal of further increasing ablation plume collection and/or controlling evaporative loss. The Omni slide planar substrate was substituted with a quarter-inch glass capillary ampoule filled with several hundred microliters of sample solution. Keeping the cross union temperature below 250 °C, the sample-loaded ampoule was inserted at the bottom cross union joint and held in place by system vacuum. With this sampling strategy, uptake of aerosols generated in the ablation plume was maximized, allowing heavier ejecta to be recycled upon recapture in the capillary reservoir.

Figure 6a depicts the LA-VaPI spectrum obtained from an aqueous PEG solution, showing uniform ion intensity and

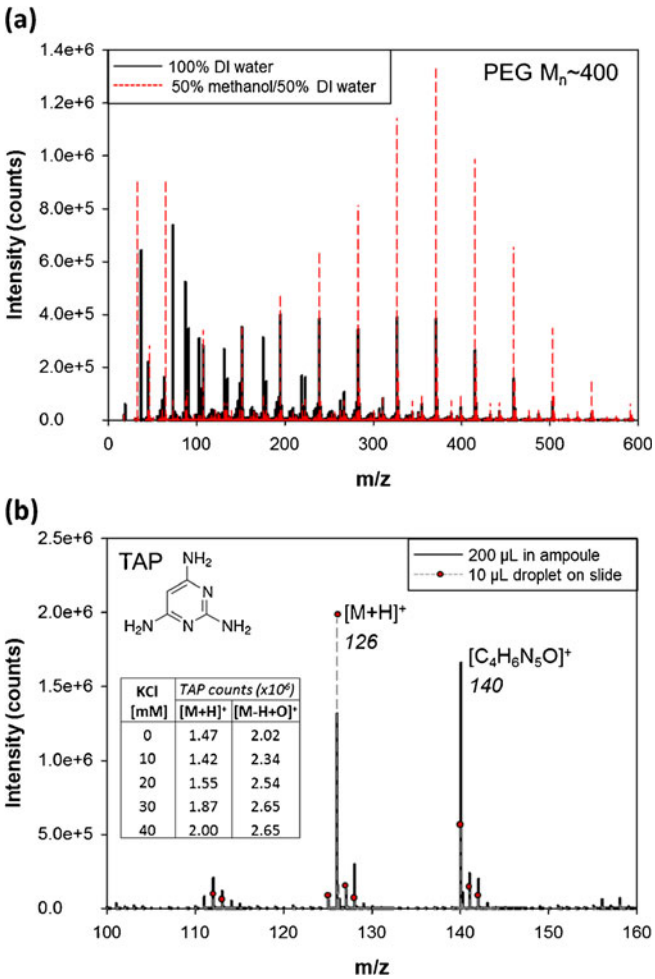

Figure 6. Investigation of matrix effects using LA-VaPI with 20 W DC discharge and 1.6 LPM helium. Mass spectra for ~4 mg mL^{-1} PEG standard (M_n ~400) in 100% aqueous solution (black trace) and 50:50 methanol/water (red trace) **(a)**. Mass spectrum of 2.5 mM TAP in deionized water sampled from 200 µL of solution in ampoule (black trace) or 10 µL droplet on glass substrate (dotted gray trace) **(b)**. Table includes signal intensity of ions detected for 2.5 mM TAP in aqueous solution as a function of KCl molar concentration ablating from ampoule. Unless otherwise specified, ablation was performed from 200 µL solution in capillary ampoule held by vacuum in the cross union heated to ~200 °C. Laser wavelength, frequency, and effective energy were 2940 nm, 10 Hz, and ~1 mJ. Spectra and bar graph intensities were extracted from 1 min average of stable TIC signal

polymer unit spacing. Interestingly, both analyte signal intensity and peak distribution were enhanced by addition of organic solvent to the aqueous matrix solution (red dotted trace). Not only was the net signal significantly higher for polymer analytes ablated from the mixed solvent system, but the $[M+H]^+$ peak distribution more accurately reflected the PEG polydispersity ($M_n = 395–410$). It is conjectured that the higher organic solvent content facilitated aerosol plume formation by changing the droplet size distribution [44] and the degree of analyte enrichment, which in turn promoted more facile desolvation/ionization in the afterglow region. Experiments with methanol concentrations in the 20%–90% range showed largely similar results.

LA-VaPI also proved relatively resistant to the negative effects associated with high salt concentrations in the sample medium. For example, LA-VaPI was used to analyze solutions containing both potassium chloride and 2,4,6-triamidopyrimidine (TAP), a nucleobase analogue involved in noncovalent self-assembly structures with cyanuric acid that are stabilized by cationic salts in aqueous solution [45]. For KCl concentrations up to 40 mM, the average TAP signal was relatively unaffected (inset table, Figure 6b), with a moderate signal enhancement as salt concentrations increased. Similar to the effect of organic solvent on PEG signal, concentrated salt ions in the aqueous matrix may influence analyte solubility and droplet distribution to promote volatilization.

Mass spectra showing the two TAP analytes detected using the different LA-VaPI sampling approaches are overlaid in Figure 6b. The protonated TAP monomer and an additional TAP derivative with accurate mass $m/z = 140.0583$ and formula $[C_4H_6N_5O]^+$ (alternatively denoted as $[TAP-H+O]^+$) are present in varying proportions. Reactant ions including N_2^+, O^+/O_2^+, and NO^+ have been commonly reported for ambient helium discharge sources like FAPA [5] and PADI [19]. Although far less abundant than the reactant $(H_2O)_nH^+$ series, the peak intensity for NO^+ was observed to increase (more than double) in the background spectrum using the enclosed ampoule sampling method because of enhanced diffusion of atmospheric N_2 and O_2 into the discharge. This same exposure to the plasma corresponded to an increase of the TAP byproduct ion ($m/z = 140$) relative to the protonated monomer ($m/z = 126$). Again, this effect was not an anomaly. As witnessed previously for 2,4-lutidine, a minor byproduct identified as $[M-H+O]^+$ was seen at $m/z = 122$ using TM-VaPI, and an NO^+ adduct of 2,4-lutidine was also detected at $m/z = 137$ (not shown) when sampling from the LA-VaPI ampoule. It appears that conjugated cyclic amines of the pyridine/pyrimidine structure are prone to byproduct formation when sampling with VaPI via plasma oxidation.

Application of LA-VaPI to Reaction Product Screening

Model prebiotic reactions studied in origins of life chemistry, such as the Miller-Urey experiment [46, 47] or the formamide reaction [48], generate highly complex, seemingly intractable mixtures [49]. In these systems, the products of interest are often not the most abundant, and product loss can propagate during sample cleanup with chromatography or extraction steps. Successful MS analysis of such mixtures necessitates sensitive instrumentation and efficient sampling measures that are robust to matrix effects. LA-VaPI was used to monitor natural and alternative nucleobase products formed in formamide and pyrazine model prebiotic reactions. The synthetic pathways postulated for the formamide reaction have been reviewed in the literature [48, 50, 51], and the reaction pathway for the predicted pyrazine products is outlined by Scheme 1 in supporting information. Basic sample preparation involved collecting portions of the crude product or fractions of the desalted mixture (see the Experimental section for details), followed by resuspension in DI water and filtration to remove large particulates prior to laser ablation from the sample ampoule. In Supplementary Figure S9a, the nucleobases predicted to form in the formamide reaction, including purine, adenine, and cytosine, were all identified for a reaction run to completion (120 h at 160 °C). Analyzing the same reaction after only 72 h, purine was still seen as the prevailing nucleobase, but the spectrum was also dominated by low mass species involving the volatile formamidine precursor, and adenine and cytosine were far less abundant. Supplementary Figure S9b shows a spectrum for a reaction mixture containing 2-aminopyrazine products. The desired 5(6)-dinydroxypropyl-2-aminopyridine compound at $m/z = 170$ was barely observable above the noise threshold, but appreciable amounts of other pyrazine products were detected, including the protonated monomers of 5-methyl-2-pyrazinamine and 5-amino-2-pyrazineethanol at $m/z = 110$ and $m/z = 140$, respectively. A possible reaction byproduct of the glycine amidine reagent was also copiously present and identified with the formula $[C_4H_7N_5]^+$ based on accurate mass ($m/z = 125.0702$).

Conclusions

The VaPI source is a highly modular design featuring complementary sampling techniques, readily adaptable to a number of sampling scenarios and directly compatible with modern instrument inlets incorporating glass transfer capillaries. Acquiring reproducible, quantitative signals with TM-VaPI or LA-VaPI depends on a balance between source gas temperature and helium flow rate, which ultimately govern the vacuum pressure dynamics within the cross union and determine the available reactant ion population. To this effect, differences in analyte signal intensity observed between equivalent power AC and DC discharges were linked to subtle variations in temperature between power regimes rather than differences in active metastable concentration. As demonstrated, the VaPI source is amenable to analyzing both solutions and solids, but both transmission and laser ablation modes can benefit from organic solvent addition during sampling to facilitate aerosol extraction and volatilization. This initial investigation of VaPI promises to inspire additional modalities in future work, such

as TM-VaPI combined with solid phase micro-extraction sample meshes, LA-VaPI from thin-layer chromatography substrates, direct infusion extractive spray (ES)-VaPI for online reaction monitoring, and microchip surface acoustic wave nebulization (SAWN)-VaPI.

Acknowledgments

The authors acknowledge support for his study by the NSF and NASA Astrobiology Program under the NSF Center for Chemical Evolution (CHE-1004570).

References

1. Cody, R.B., Laramée, J.A., Durst, H.D.: Versatile new ion source for the analysis of materials in open air under ambient conditions. Anal. Chem. **77**, 2297–2302 (2005)
2. Harper, J.D., Charipar, N.A., Mulligan, C.C., Zhang, X., Cooks, R.G., Ouyang, Z.: Low-temperature plasma probe for ambient desorption ionization. Anal. Chem. **80**, 9097–9104 (2008)
3. Ratcliffe, L.V., Rutten, F.J.M., Barrett, D.A., Whitmore, T., Seymour, D., Greenwood, C.: Surface analysis under ambient conditions using plasma-assisted desorption/ionization mass spectrometry. Anal. Chem. **79**, 6094–6101 (2007)
4. Salter, T.L., Gilmore, I.S., Bowfield, A., Olabanji, O.T., Bradley, J.W.: Ambient surface mass spectrometry using plasma-assisted desorption ionization: effects and optimization of analytical parameters for signal intensities of molecules and polymers. Anal. Chem. **85**, 1675–1682 (2013)
5. Andrade, F.J., Shelley, J.T., Wetzel, W.C., Webb, M.R., Gamez, G., Ray, S.J.: Atmospheric pressure chemical ionization source. 1. Ionization of compounds in the gas phase. Anal. Chem. **80**, 2646–2653 (2008)
6. Andrade, F.J., Shelley, J.T., Wetzel, W.C., Webb, M.R., Gamez, G., Ray, S.J.: Atmospheric pressure chemical ionization source. 2. Desorption-ionization for the direct analysis of solid compounds. Anal. Chem. **80**, 2654–2663 (2008)
7. Na, N., Zhang, C., Zhao, M., Zhang, S., Yang, C., Fang, X.: Direct detection of explosives on solid surfaces by mass spectrometry with an ambient ion source based on dielectric barrier discharge. J. Mass Spectrom. **42**, 1079–1085 (2007)
8. Nilles, J.M., Connell, T.R., Stokes, S.T., Dupont Durst, H.: Explosives detection using direct analysis in real time (DART) mass spectrometry. Propell. Explosive. Pyrotech. **35**, 446–451 (2010)
9. Gilbert-Lopez, B., Garcia-Reyes, J.F., Meyer, C., Michels, A., Franzke, J., Molina-Diaz, A.: Simultaneous testing of multiclass organic contaminants in food and environment by liquid chromatography/dielectric barrier discharge ionization-mass spectrometry. Analyst **137**, 5403–5410 (2012)
10. Grange, A.H.: Semiquantitative analysis of contaminants in soils by direct analysis in real time (DART) mass spectrometry. Rapid Commun. Mass Spectrom. **27**, 305–318 (2013)
11. Ma, X., Zhang, S., Lin, Z., Liu, Y., Xing, Z., Yang, C.: Real-time monitoring of chemical reactions by mass spectrometry utilizing a low-temperature plasma probe. Analyst **134**, 1863–1867 (2009)
12. Hajslova, J., Cajka, T., Vaclavik, L.: Challenging applications offered by direct analysis in real time (DART) in food-quality and safety analysis. TrAC Trend. Analy. Chem. **30**, 204–218 (2011)
13. Fernandez, F.M., Cody, R.B., Green, M.D., Hampton, C.Y., McGready, R., Sengaloundeth, S.: Characterization of solid counterfeit drug samples by desorption electrospray ionization and direct-analysis-in-real-time coupled to time-of-flight mass spectrometry. Chem. Med. Chem. **1**, 702–705 (2006)
14. Liu, Y., Lin, Z., Zhang, S., Yang, C., Zhang, X.: Rapid screening of active ingredients in drugs by mass spectrometry with low-temperature plasma probe. Anal. Bioanal. Chem. **395**, 591–599 (2009)
15. Brewer, T.M., Verkouteren, J.R.: Atmospheric identification of active ingredients in over-the-counter pharmaceuticals and drugs of abuse by atmospheric pressure glow discharge mass spectrometry (APGD-MS). Rapid Commun. Mass Spectrom. **25**, 2407–2417 (2011)
16. Zhou, M., McDonald, J.F., Fernandez, F.M.: Optimization of a direct analysis in real time/time-of-flight mass spectrometry method for rapid serum metabolomic fingerprinting. J. Am. Soc. Mass Spectrom. **21**, 68–75 (2010)
17. Jones, C.M., Fernandez, F.M.: Transmission mode direct analysis in real time mass spectrometry for fast untargeted metabolic fingerprinting. Rapid Commun. Mass Spectrom. **27**, 1311–1318 (2013)
18. Kratzer, J., Mester, Z., Sturgeon, R.E.: Comparison of dielectric barrier discharge, atmospheric pressure radiofrequency-driven glow discharge and direct analysis in real time sources for ambient mass spectrometry of acetaminophen. Spectrochim. Acta B Atom. Spectroscop. **66**, 594–603 (2011)
19. McKay, K., Salter, T.L., Bowfield, A., Walsh, J.L., Gilmore, I.S., Bradley, J.W.: Comparison of three plasma sources for ambient desorption/ionization mass spectrometry. J. Am. Soc. Mass Spectrom. **25**, 1528–1537 (2014)
20. Chan, G.C.Y., Shelley, J.T., Wiley, J.S., Engelhard, C., Jackson, A.U., Cooks, R.G.: Elucidation of reaction mechanisms responsible for afterglow and reagent-ion formation in the low-temperature plasma probe ambient ionization source. Anal. Chem. **83**, 3675–3686 (2011)
21. Song, L., Gibson, S.C., Bhandari, D., Cook, K.D., Bartmess, J.E.: Ionization mechanism of positive-ion direct analysis in real time: a transient microenvironment concept. Anal. Chem. **81**, 10080–10088 (2009)
22. Danhelova, H., Hradecky, J., Prinosilova, S., Cajka, T., Riddellova, K., Vaclavik, L.: Rapid analysis of caffeine in various coffee samples employing direct analysis in real-time ionization-high-resolution mass spectrometry. Anal. Bioanal. Chem. **403**, 2883–2889 (2012)
23. Gilbert-Lopez, B., Geltenpoth, H., Meyer, C., Michels, A., Hayen, H., Molina-Diaz, A.: Performance of dielectric barrier discharge ionization mass spectrometry for pesticide testing: a comparison with atmospheric pressure chemical ionization and electrospray ionization. Rapid Commun. Mass Spectrom. **27**, 419–429 (2013)
24. Zhao, Y., Lam, M., Wu, D., Mak, R.: Quantification of small molecules in plasma with direct analysis in real time tandem mass spectrometry, without sample preparation and liquid chromatographic separation. Rapid Commun. Mass Spectrom. **22**, 3217–3224 (2008)
25. Harris, G., Falcone, C., Fernández, F.: Sensitivity "hot spots" in the direct analysis in real time mass spectrometry of nerve agent simulants. J. Am. Soc. Mass Spectrom. **23**, 153–161 (2012)
26. Harris, G.A., Fernandez, F.M.: Simulations and experimental investigation of atmospheric transport in an ambient metastable-induced chemical ionization source. Anal. Chem. **81**, 322–329 (2009)
27. Pfeuffer, K.P., Ray, S.J., Hieftje, G.M.: Measurement and visualization of mass transport for the flowing atmospheric pressure afterglow (FAPA) ambient mass-spectrometry source. J. Am. Soc. Mass. Spectrom. **25**, 800–808 (2014)
28. Pfeuffer, K.P., Shelley, J.T., Ray, S.J., Hieftje, G.M.: Visualization of mass transport and heat transfer in the FAPA ambient ionization source. J. Anal. At. Spectrom. **28**, 379–387 (2013)
29. Curtis, M., Keelor, J.D., Jones, C.M., Pittman, J.J., Jones, P.R., Sparkman, O.D.: Schlieren visualization of fluid dynamics effects in direct analysis in real time mass spectrometry. Rapid Commun. Mass Spectrom. **29**, 431–439 (2015)
30. Yu, S., Crawford, E., Tice, J., Musselman, B., Wu, J.-T.: Bioanalysis without Sample cleanup or chromatography: the evaluation and initial implementation of direct analysis in real time ionization mass spectrometry for the quantification of drugs in biological matrixes. Anal. Chem. **81**, 193–202 (2009)
31. Häbe, T.T., Morlock, G.E.: Quantitative surface scanning by direct analysis in real time mass spectrometry. Rapid Commun. Mass Spectrom. **29**, 474–484 (2015)
32. Gilbert-López, B., Schilling, M., Ahlmann, N., Michels, A., Hayen, H., Molina-Díaz, A.: Ambient diode laser desorption dielectric barrier discharge ionization mass spectrometry of nonvolatile chemicals. Anal. Chem. **85**, 3174–3182 (2013)
33. Feng, B., Zhang, J., Chang, C., Li, L., Li, M., Xiong, X.: Ambient mass spectrometry imaging: plasma assisted laser desorption ionization mass spectrometry imaging and its applications. Anal. Chem. **86**, 4164–4169 (2014)
34. Shelley, J.T., Ray, S.J., Hieftje, G.M.: Laser ablation coupled to a flowing atmospheric pressure afterglow for ambient mass spectral imaging. Anal. Chem. **80**, 8308–8313 (2008)
35. Chen, L.C., Yu, Z., Furuya, H., Hashimoto, Y., Takekawa, K., Suzuki, H.: Development of ambient sampling chemi/chemical ion source with dielectric barrier discharge. J. Mass Spectrom. **45**, 861–869 (2010)
36. Nudnova, M.M., Zhu, L., Zenobi, R.: Active capillary plasma source for ambient mass spectrometry. Rapid Commun. Mass Spectrom. **26**, 1447–1452 (2012)

37. Ewing, R.G., Clowers, B.H., Atkinson, D.A.: Direct real-time detection of vapors from explosive compounds. Anal. Chem. **85**, 10977–10983 (2013)
38. Dixon, R.B., Sampson, J.S., Hawkridge, A.M., Muddiman, D.C.: Ambient aerodynamic ionization source for remote analyte sampling and mass spectrometric analysis. Anal. Chem. **80**, 5266–5271 (2008)
39. Dwivedi, P., Gazda, D.B., Keelor, J.D., Limero, T.F., Wallace, W.T., Macatangay, A.V.: Electro-thermal vaporization direct analysis in real time-mass spectrometry for water contaminant analysis during space missions. Anal. Chem. **85**, 9898–9906 (2013)
40. Schaper, J.N., Pfeuffer, K.P., Shelley, J.T., Bings, N.H., Hieftje, G.M.: Drop-on-demand sample introduction system coupled with the flowing atmospheric-pressure afterglow for direct molecular analysis of complex liquid microvolume samples. Anal. Chem. **84**, 9246–9252 (2012)
41. Reininger, C., Woodfield, K., Keelor, J.D., Kaylor, A., Fernández, F.M., Farnsworth, P.B.: Absolute number densities of helium metastable atoms determined by atomic absorption spectroscopy in helium plasma-based discharges used as ambient desorption/ionization sources for mass spectrometry. Spectrochim. Acta B Atom. Spectroscop. **100**, 98–104 (2014)
42. Vandercruyssen, K., D'Hondt, M., Vergote, V., Jansen, H., Burvenich, C., De Spiegeleer, B.: LC-UV/MS quality analytics of paediatric artemether formulations. J. Pharmaceut. Anal. **4**, 37–52 (2014)
43. Na, N., Zhao, M., Zhang, S., Yang, C., Zhang, X.: Development of a dielectric barrier discharge ion source for ambient mass spectrometry. J. Am. Soc. Mass Spectrom. **18**, 1859–1862 (2007)
44. Green, F.M., Salter, T.L., Gilmore, I.S., Stokes, P., O'Connor, G.: The effect of electrospray solvent composition on desorption electrospray ionisation (DESI) efficiency and spatial resolution. Analyst **135**, 731–737 (2010)
45. Chen, M.C., Cafferty, B.J., Mamajanov, I., Gállego, I., Khanam, J., Krishnamurthy, R.: Spontaneous prebiotic formation of a β-ribofuranoside that self-assembles with a complementary heterocycle. J. Am. Chem. Soc. **136**, 5640–5646 (2014)
46. Parker, E.T., Zhou, M., Burton, A.S., Glavin, D.P., Dworkin, J.P., Krishnamurthy, R.: A plausible simultaneous synthesis of amino acids and simple peptides on the primordial earth. Angew. Chem. Int. Ed. **53**, 8132–8136 (2014)
47. McCollom, T.M.: Miller-Urey and beyond: what have we learned about prebiotic organic synthesis reactions in the past 60 years? Annu. Rev. Earth Planet. Sci. **41**, 207–229 (2013)
48. Hudson, J.S., Eberle, J.F., Vachhani, R.H., Rogers, L.C., Wade, J.H., Krishnamurthy, R.: A unified mechanism for abiotic adenine and purine synthesis in formamide. Angew. Chem. Int. Ed. **51**, 5134–5137 (2012)
49. Schwartz, A.W.: Intractable mixtures and the origin of life. Chem. Biodiv. **4**, 656–664 (2007)
50. Wang, J., Gu, J., Nguyen, M.T., Springsteen, G., Leszczynski, J.: From formamide to purine: a self-catalyzed reaction pathway provides a feasible mechanism for the entire process. J. Phys. Chem. B **117**, 9333–9342 (2013)
51. Nguyen, H.T., Jeilani, Y.A., Hung, H.M., Nguyen, M.T.: Radical pathways for the prebiotic formation of pyrimidine bases from formamide. J. Phys. Chem. A **119**, 8871–8883 (2015)